Environmental Science & Technology

pubs.acs.org/est

Article

Redispersion Behavior of 2D MoS_2 Nanosheets: Unique Dependence on the Intervention Timing of Natural Organic Matter

Bei Liu, Zixin Han, Qi Han, Yufei Shu, Li Li, Beizhao Chen, Zhongying Wang,* and Joel A. Pedersen*

Cite This: https://doi.org/10.1021/acs.est.2c05282

Read Online

ACCESS | Metrics & More | Article Recommendations | Supporting Information

ABSTRACT: The aggregation−redispersion behavior of nanomaterials determines their transport, transformation, and toxicity, which could be largely influenced by the ubiquitous natural organic matter (NOM). Nonetheless, the interaction mechanisms of two-dimensional (2D) MoS_2 and NOM and the subsequent influences on the redispersion behavior are not well understood. Herein, we investigated the redispersion of single-layer MoS_2 (SL-MoS_2) nanosheets as influenced by Suwannee River NOM (SRNOM). It was found that SRNOM played a decisive role on the redispersion of MoS_2 2D nanosheets that varied distinctly from the 3D nanoparticles. Compared to the poor redispersion of MoS_2 aggregates in the absence or post-addition of SRNOM to the aggregates, co-occurrence of SRNOM in the dispersion could largely enhance the redispersion and mobility of MoS_2 by intercalating into the nanosheets. Upon adsorption to SL-MoS_2, SRNOM enhanced the hydration force and weakened the van der Waals forces between nanosheets, leading to the redispersion of the aggregates. The SRNOM fractions with higher molecular mass imparted better dispersity due to the preferable sorption of the large molecules onto SL-MoS_2 surfaces. This comprehensive study advances current understanding on the transport and fate of nanomaterials in the water system and provides fresh insights into the interaction mechanisms between NOM and 2D nanomaterials.

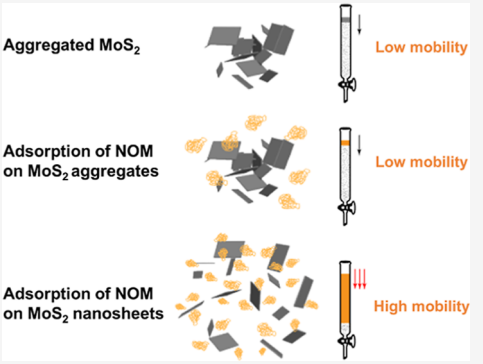

KEYWORDS: *two-dimensional nanomaterials, transition metal dichalcogenides (TMDs), transformation, aggregation, redispersion*

INTRODUCTION

Molybdenum disulfide (MoS_2) is one of the most widely researched two-dimensional (2D) transition metal dichalcogenides for its distinguished properties, which has been reported for applications in biomedical, electronics, catalysis, and environmental fields.[1−5] The increasing usage will lead to elevated occurrences of the MoS_2 materials in the environment, raising concerns over their potential risks to human health and the environment.[6−8] Similar to many other nanomaterials, environmental conditions under which the primary nanosized materials remain as discrete units or aggregate into clusters will dictate their environmental fate and transport and thus potential ecotoxicological impacts.[9,10] Therefore, we find it critical to acquire the understandings concerning the aggregation and redispersion behavior of MoS_2 nanomaterials as influenced by environmental conditions to fully understand the transformation and potential toxicity of the nanomaterials.

Natural organic matter (NOM) is ubiquitous in natural environments, which constitutes the largest portion of the organic content in soil and water systems.[11,12] Nanomaterials in natural waters, regardless of size, would interact with these organic macromolecules that alter the nanomaterials' stability and other characteristics. The presence of NOM is anticipated to play a key role on the colloidal stabilities of nanomaterials.[13] NOM can either induce the aggregation of positively charged nanoparticles by neutralizing nanomaterials charge[14,15] or stabilize the nanomaterials through electrostatic repulsion or steric hindrance effects[16,17] due to the negatively charged carboxylic and phenolic moieties. The specific consequence and extent depends on the surface charge of nanomaterials, content of NOM as well as NOM properties.[18−20] Under environmental conditions, NOM could also be adsorbed on the surface of nanomaterials.[21−23] The acquisition of a NOM "corona" modifies the physicochemical characteristics of the solid−water interface and thus has substantial influences on the fate, transport, and even toxicity of nanomaterials.[24,25] For example, acquisition of the NOM layer on the nanoparticles assisted the transport of nanoparticles in porous media;[26] due to the sorption of NOM, the attachment of nanomaterials on the cell membrane were impacted and thus altered the toxicity to cells.[14,27]

Received: July 21, 2022
Revised: December 1, 2022
Accepted: December 1, 2022

Concerning the aggregation behavior of MoS_2, previous studies have addressed the colloidal stability of MoS_2, which was found to be influenced by its physiochemical properties and environmental factors, including pH, ionic strength, and light irradiation.[28−30] Until now, however, the interaction of 2D MoS_2 nanosheets and NOM is far from well understood. Although previous studies have reported the phenomenon that the presence of NOM could inhibit the homo- and hetero-aggregation of MoS_2 nanosheets,[31,32] a research gap existed with respect to the interaction of MoS_2 and NOM as influenced by their respective properties. Unlike the intensively studied positively charged nanomaterials or organic materials which could associate with NOM through electrostatic attraction, $\pi-\pi$ interaction, or hydrogen bonding,[33,34] the sorption of NOM onto negatively charged inorganic MoS_2 nanomaterials remain largely unknown. The interaction mechanism exploration is expected to have board implications for the nanomaterials' behavior prediction in aquatic systems where most particles, porous media, and NOM have negative charges. Moreover, most consideration in the previous works was given to the influence of the NOM on aggregation process, with the aggregation kinetics and sedimentation of these coated particles having been shown;[5,6,12,27,28] yet the reverse process from the aggregated states back to the dispersed state (i.e., redispersion) is often overlooked. In fact, redispersion of nanomaterials determines if nanomaterials could reacquire mobility or even bioavailability and toxicity when the environmental condition changed to the aggregation unfavorable condition. Some studies have reported the reversible aggregation of 3D nanoparticles and disaggregation in the presence of NOM,[35−37] whereas the redispersion behavior of 2D nanosheets could be varied because of the distinct morphologies and has not been revealed to the best of our knowledge. Overall, identification of the redispersion behavior of MoS_2 nanosheets under different conditions and impacts of NOM are needed to better elucidate the transport and fate of 2D nanomaterials.

In the present study, single-layer MoS_2 (SL-MoS_2) nanosheets were prepared via chemical exfoliation to explore the aggregation and redispersion behavior of MoS_2, with an emphasis on revealing the role of NOM on the redispersion of the nanosheets. Aggregates of SL-MoS_2 in the absence and presence of NOM were extensively characterized to determine the effects of NOM on the structure, morphology, and surface chemistry of SL-MoS_2. Finally, to elucidate the interaction mechanism, the sorption was evaluated by using the nanosheets with varying hydrophilicity and NOM with different molecular weights (MWs), which were obtained through MoS_2 phase transformation and sequential fractionation, respectively. This study is expected to provide novel insights into the role of organic macromolecules on the remobilization of nanomaterials.

MATERIALS AND METHODS

SL-MoS_2 Nanosheet Exfoliation and Phase Transformation. Chemicals and their purities and supplies are reported in the Supporting Information (Text S1). A colloidal suspension of SL-MoS_2 nanosheets was prepared through Li intercalation and exfoliation of commercial MoS_2 powder (2 μm, Sigma-Aldrich), followed by extensive purification as described in the Supporting Information (Text S2).[38] To obtain the nanosheets with different hydrophilicities, transformed SL-MoS_2 nanosheets with varying phase composition were obtained by pressurized hydrothermal treatment of the as-exfoliated SL-MoS_2 suspension in N_2.[39] Specifically, 20 mL of a ∼500 mg/L SL-MoS_2 suspension was deoxygenated in a N_2-filled glovebox, added to a Teflon-lined autoclave (50 mL volume, Wenbo Experimental Instrument Co., Ltd) and then heated at 120, 150, and 200 °C for 2 h (referred to as SL-120, SL-150, SL-200, respectively, and SL-pristine for the as-exfoliated MoS_2). The concentration of SL-MoS_2 stock solution was accurately determined by digestion in a 0.2 M HNO_3 and 0.5 M H_2O_2 solution, followed by the measurement of the soluble Mo concentration by an inductively coupled plasma−optical emission spectrometer (iCAP 7400, Thermo Scientific). The pristine and transformed SL-MoS_2 nanosheets were kept in the N_2-filled glovebox for future use.

NOM Solution Preparation and Fractionation. Suwannee River NOM (SRNOM) was obtained from the International Humic Substances Society (1R101N, St. Paul, MN). Stock solutions of SRNOM (2000 mg/L) were prepared in ultrapure water (≥18.2 MΩ·cm resistivity, Millipore) and adjusted to pH 10 with 1 M NaOH. To ensure the complete dissolution, the stock solution was allowed to stir overnight in the dark, filtered through a 0.22 μm Teflon filter, and stored at 4 °C.

NOM was fractionated based on the MW distribution by using a series of Amicon Ultra-15 centrifugal filters (EMD Millipore) with different MW cutoffs (MWCOs) of 100, 30, 10, and 3 kDa, as described previously.[15] Briefly, all filter units were pre-rinsed by centrifuging at 4000g (3K15, Sigma) with 10 mL of ultrapure water three times. The SRNOM suspension was subjected to sequential fractionation, with the filtrate from each higher MWCO filter being utilized in the following step of filtration. In each step, the retentate fractions were rinsed in the filter unit with ultrapure water to remove any remaining NOM with lower MW until the filtrate showed minimal observable color. Finally, the concentrated retentate was collected, namely, SRNOM fractions of >100, 30−100, 10−30, 3−10, and <3 kDa. The mass concentration of each fraction was determined as total organic carbon (TOC) using a TOC analyzer (Multi N/C 3100, Jena). The cumulative mass recovery across the entire sequential filtration was ∼97%. All stock solutions of fractionated and pristine SRNOM were stored in the dark at 4 °C and diluted for future use.

Aggregation and Redispersion of SL-MoS_2. To obtain the preliminary understanding for the redispersion behavior of SL-MoS_2, the aggregates were formed in the solution with high ionic strength. Based on our previous work, the critical coagulation concentration of Ca^{2+} to induce the fast aggregation of SL-MoS_2 is 0.9 mM.[28] Therefore, a higher concentration of 2 mM Ca^{2+} was chosen in this study to ensure the rapid aggregation and sedimentation of SL-MoS_2. For redispersion, the as-deposited aggregates were collected by centrifugation, followed by transferring to the ultrapure water, which represents the condition with low ionic strength favored by disaggregation. After vortex shaking at 2500 rpm (VERTEX 3, IKA) for 1 min, the z-averaged hydrodynamic diameter (D_h) of the redispersion was recorded using dynamic light scattering (DLS; Nanosizer, NanoBrook Omni, Brookhaven) and compared to the pristine dispersion to evaluate if the aggregation is reversible. To highlight the unique behavior of 2D nanosheets, the flower-like MoS_2 nanoparticles were synthesized as described previously,[40] which were identical in chemical composition with SL-MoS_2 (Figure S1), and subjected to the similar aggregation−redispersion process. As

https://doi.org/10.1021/acs.est.2c05282
Environ. Sci. Technol. XXXX, XXX, XXX−XXX

references, the redispersion of other commonly researched nanoparticles (TiO_2, CeO_2, and Al_2O_3) was conducted at pH 4 where the nanoparticles are highly charged (Figure S2).

To quantify the role of NOM on the aggregation and redispersion, a mixture of SL-MoS_2 suspension (10 mg/L) and SRNOM at desired concentrations (0, 2, 5, 10, 20, and 50 mg/L) was prepared by diluting the exfoliated MoS_2 and NOM stock solutions with 3.4 mM phosphate buffer composting of 3.37 mM NaH_2PO_3 and 0.03 mM Na_2HPO_3 (pH 5.0). Electrolyte solution of $CaCl_2$ (2 mM) or NaCl (200 mM) was added to the mixture of MoS_2 and SRNOM to induce the aggregation of MoS_2 nanosheets. To study the influence of SRNOM on the aggregation kinetics, time-resolved DLS was used to measure the D_h of SL-MoS_2 nanosheets. The sedimentation process was quantified by measuring the absorbance at 450 nm to quantify the remaining MoS_2 concentration in the suspension. In the presence of SRNOM, the sedimentation rate of SL-MoS_2 nanosheets induced by Ca^{2+} was significantly slowed down (Figure S3), while the complete sedimentation (A_{450} < 0.1) was approached after 24 h. After complete sedimentation, the suspension was subjected to centrifugation at 3000g for 5 min, and the supernatant was replaced by equivalent Milli-Q water. The redispersion process was initiated by vortex shaking for 1 min followed by centrifugation at 3000g to remove the undispersed fraction. Given the good linear relationship between the absorbance and MoS_2 concentration in supernatant (Figure S4), the redispersion efficiency was determined as

$$\text{efficiency} = \frac{A_r}{A_0} \times 100\%$$

where A_r and A_0 is the absorbance at 450 nm of the redispersion and the dispersion before aggregation, respectively. Size distribution of the redispersed suspension was recorded by DLS. To elucidate weather the redispersion of SL-MoS_2 nanosheets depends on the NOM intervention timing, SRNOM was added to the dispersion before or after the aggregates' formation (co-addition vs post-addition to Ca^{2+}, Figure S5). Column experiment was conducted to evaluate transport of the nanosheets in the absence or presence of NOM (Text S3).

Adsorption of SRNOM onto SL-MoS_2 Nanosheets. The adsorption of SRNOM onto SL-MoS_2 nanosheets was studied by batch experiments. Briefly, the phosphate buffer solution (3.4 mM) was used to keep the solution at a constant pH of 5.0. A series of Ca^{2+} (0−20 mM) or Na^+ (0−800 mM) solutions were added to the mixture of SL-MoS_2 (10 mg/L) and SRNOM (20 mg/L) to investigate the sorption as a function of cation concentration. To obtain the SRNOM sorption isotherm, SL-MoS_2 suspension in the concentration of 10 mg/L was mixed with SRNOM in a series of concentrations at 0, 2, 5, 10, 20, 30, and 50 mg/L. The isotherms were compared between different nanosheets (SL-Pristine, SL-120, SL-150, and SL-200) to explore the affinity as a function of nanomaterial properties. The background electrolyte was either 2 mM $CaCl_2$ or 200 mM NaCl. In contrast to the pre-mix of SL-MoS_2 and SRNOM prior to the addition of Ca^{2+} (i.e., SRNOM co-addition), SRNOM post-addition to MoS_2 aggregate experiments were conducted to distinguish the sorption of SRNOM by MoS_2 nanosheets or aggregates. Briefly, 2 mM Ca^{2+} was added to the MoS_2 suspension without SRNOM, and the suspension stood still for 10 h to allow complete sedimentation, followed by the addition of SRNOM in different concentrations. The NOM-mixed MoS_2 aggregate suspension was standing at room temperature for 24 h to reach the adsorption equilibrium (Figure S6). The adsorbed NOM by SL-MoS_2 aggregates was removed through centrifuge (8000g, 5 min), followed by filtration through 0.22 μm PES syringe filters.

Ultraviolet−visible (UV−vis) absorption spectroscopy was used to determine the amount of chromophoric SRNOM bound to the surface of MoS_2. The concentration of SRNOM remaining in the supernatant was quantified by comparing the absorbance at 254 nm to a calibration curve made from a stock SRNOM solution (Figure S7).[41] Although it is a widely used method, it should be noted that it might result in an overestimation of the adsorbed mass, due to the preferable adsorption for the aromatic species which possess higher adsorption. The equilibrium adsorption capacity Q_e (mg/g) of SRNOM to MoS_2 is calculated as

$$Q_e = \frac{V(C_0 - C_f)}{m}$$

where V is the solution volume (mL), and C_0 and C_f are the initial and final concentration of SRNOM, respectively, and m is the SL-MoS_2 mass (g). The Freundlich equation is an empirical model describing the adsorption onto a heterogeneous surface and was used to fit the adsorption isotherm as follows

$$Q_e = K_f C_f^N$$

where K_f is the Freundlich affinity coefficient, and N is the exponential coefficient.

Characterization of MoS_2 Nanosheets and Aggregates. The morphologies of pristine SL-MoS_2 nanosheets and transformed MoS_2 nanosheets were characterized by transmission electron microscopy (TEM; FEI Talos F200X microscope equipped with a Schottky emitter gun operated at 200 kV) by depositing the dispersion on a copper grid with carbon support. Atomic force microscopy (AFM; MFP-3D-Stand Alone, Asylum Research) was used to test the thickness of the nanosheet. To characterize the chemical composition of SL-MoS_2, we performed X-ray photoelectron spectroscopy (XPS) survey and high-resolution scans with a PHI 5000 VersaProbe III equipped with a monochromatic Al anode (Al Kα = 1486.7 eV) as the X-ray source. To determine the interlayer spacing of nanosheets, SL-MoS_2 was restacked by filtration of the suspension through a PES membrane (0.22 μm, Shimadzu) and the interlayer spacing was determined using grazing incident X-ray diffraction (XRD) on a Rigaku SmartLab diffractometer (Cu Kα = 1.54 Å). Water contact angle of the nanosheets were measured from the average values for 4 μL water droplets at three different positions of the stacked film (DAS25E, Kruss). Apparent zeta potentials were determined from electrophoretic motilities (Nanosizer, Nano-Brook Omni, Brookhaven), and three measurements for three replicate samples were conducted in 20 cycles. UV−vis absorption spectra of the dispersed SL-MoS_2 nanosheets and SRNOM were recorded by a UV−vis spectrophotometer (UH 5300, Hitachi). The fractionated SRNOM samples were characterized by UV−vis (10 mg_{oc}/L) and fluorescence excitation emission matrices (EEMs; Aqualog, HORIBA Scientific) (1 mg_{oc}/L).

https://doi.org/10.1021/acs.est.2c05282
Environ. Sci. Technol. XXXX, XXX, XXX−XXX

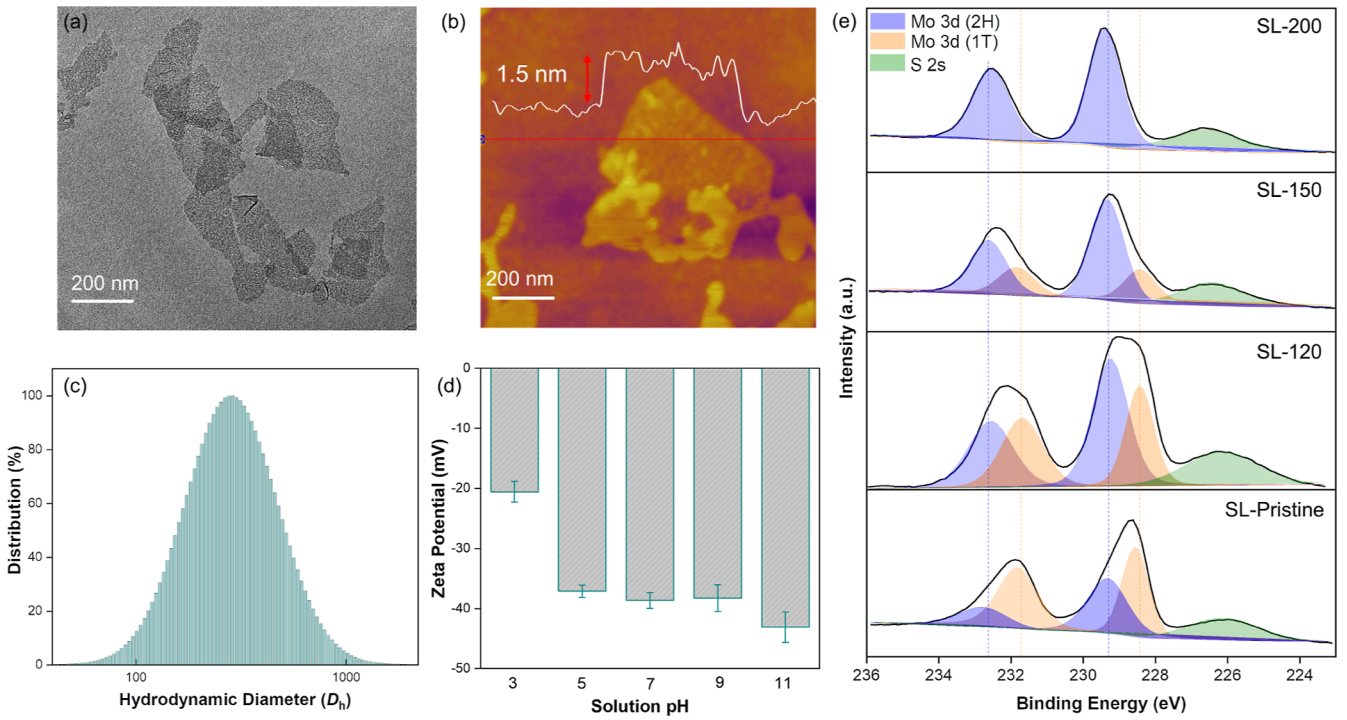

Figure 1. Characterization of SL-MoS_2 nanosheets: (a) representative TEM image; (b) representative AFM image of MoS_2 nanosheets, inset: line scan showing the thickness profile along the red line in the image; (c) *z*-averaged hydrodynamic diameter distribution determined by DLS; (d) apparent zeta potential of MoS_2 nanosheets as a function of solution pH, and (e) XPS spectra of Mo 3d and deconvolution analysis showing the increasing component of semiconducting 2H phase after transformation.

The aggregates of MoS_2 in the absence or presence of SRNOM were sampled from the suspension for TEM characterization, with the collection of energy-dispersive X-ray spectroscopy (EDS) for elemental mapping analysis and selected area electron diffraction (SAED) data. For the characterization of XPS and XRD, the aggregates were collected through filtration. To reveal the specific functional groups involved in NOM−MoS_2 interactions, attenuated total reflectance−Fourier transform infrared (ATR−FTIR) spectra of SRNOM before and after adsorbed to MoS_2 at pH 5 were recorded using a Bruker Vertex 70v FTIR Spectrometer equipped with a MCT/A detector. Spectra were recorded in the spectral range from 500 to 4000 cm^{-1} at an instrument resolution of 4 cm^{-1}.

RESULTS AND DISCUSSION

Structural Characterization and Phase Transformation of SL-MoS_2. The TEM image shows the flake-like structure of as-prepared SL-MoS_2 nanosheets in a lateral size of 100−300 nm (Figure 1a). A close observation of the nanosheets by AFM imaging reveals that the nanosheet is primarily single-layered, with the typical thickness of less than 2 nm (Figure 1b), which is consistent with monolayer MoS_2 nanosheets generated in the chemical exfoliation method.[42] The SL-MoS_2 nanosheets are highly water-dispersible with an average hydrodynamic diameter of 270 nm (Figure 1c). The colloidal stability has been attributed to the highly negative surface charge of MoS_2 nanosheets over a wide pH range (Figure 1d) imparted by the electron transfer during Li-intercalation.[43,44]

Figure 1e depicted the XPS spectra for analyzing the phase composition of as-prepared samples. The characteristic peaks of the 1T phase arising from the Mo $3d_{5/2}$ and Mo $3d_{3/2}$ orbitals were located at 228.4 and 231.6 eV, respectively, around 1 eV lower than the corresponding peaks of the 2H phase (229.4 and 232.5 eV). Deconvolution of the Mo 3d XPS spectrum reveals the phase composition of SL-pristine to be 70% 1T and 30% 2H (Figure 1e). The successful phase transformation from 1T to 2H is evident in the UV−vis spectra (Figure S8a), with the characteristic absorption bands of 2H phase turning more pronounced at 440, 610, and 670 nm.[45,46] As confirmed by the XPS analysis, the content of semiconducting 2H phase gradually increased from 30 to 50, 73, and 100% after the treatment at 120, 150, and 200 °C, respectively. We note that the transformation did not alter the single-layer morphology of nanosheets (Figure S8b) and the phase-converted nanosheets maintained well-dispersed in solutions. The transformed nanosheets displayed a similar negative charge over a large pH range (Figure S8c), slightly lower than that of SL-pristine due to the loss of the electrons during the hydrothermal treatment.

Redispersion of SL-MoS_2 in the Absence and Presence of NOM. Before the investigation on NOM effects, it is necessary to understand the intrinsic redispersion behavior of the MoS_2 nanosheets and to see if there are any differences compared to other commonly researched nanomaterials. Upon redispersion by replacing Ca^{2+}-containing supernatant with ultrapure water, the average D_h of the MoS_2 nanosheet suspension was 1.7 μm and it remained in the similar size even after stirring for 48 h (Figure 2a), suggesting the irreversible aggregation of SL-MoS_2 nanosheets. In contrast, a reversible aggregation was obtained for the flower-like MoS_2 nanoparticle, with the D_h of redispersion almost identical to the initial dispersion (Figure 2a). The results are also applicable to other common 3D nanoparticles (Al_2O_3, CeO_2, and TiO_2), which agreed well with the previous results and confirmed the

https://doi.org/10.1021/acs.est.2c05282
Environ. Sci. Technol. XXXX, XXX, XXX−XXX

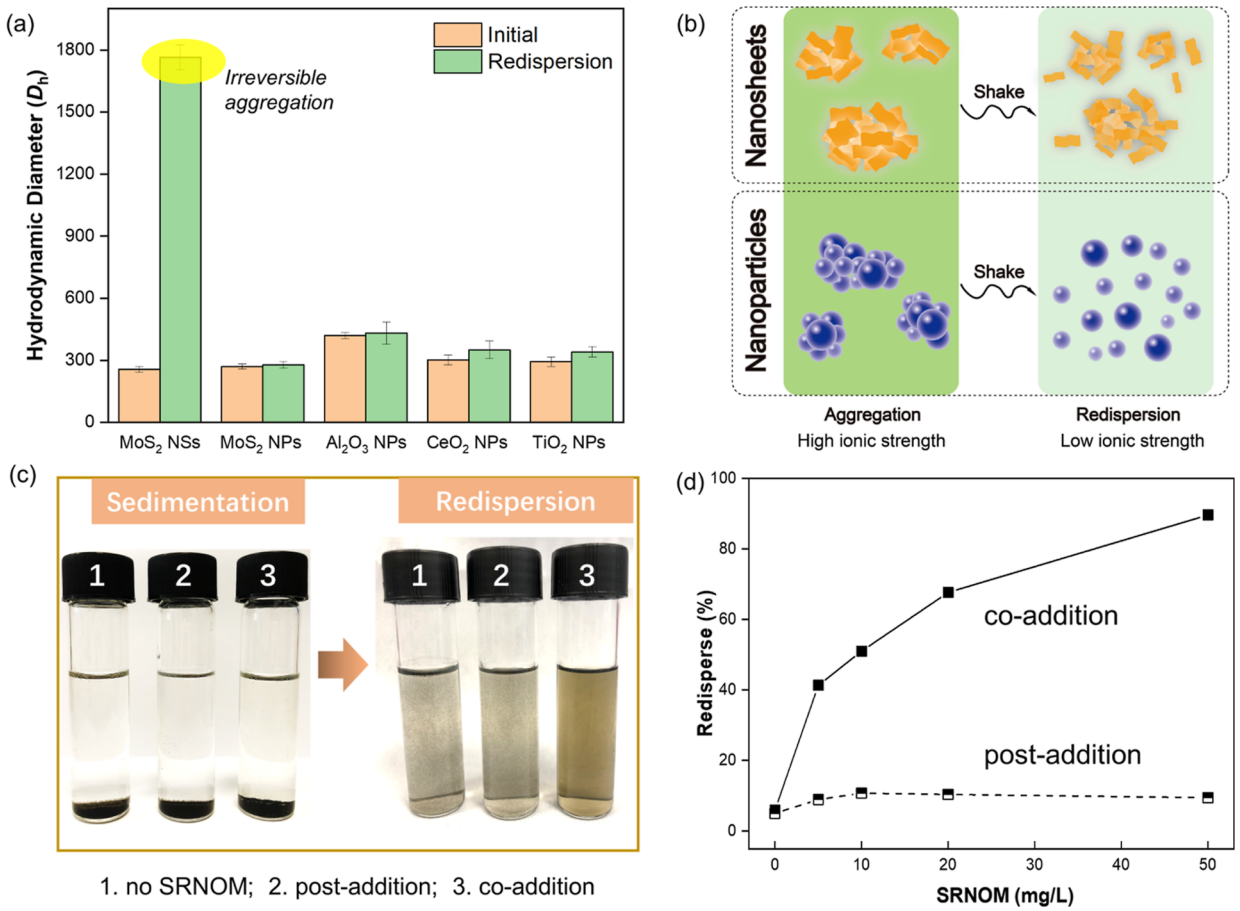

Figure 2. Redispersion of SL-MoS_2 aggregates in the absence and presence of SRNOM: (a) hydrodynamic diameter of the dispersion before aggregation and after redispersion (MoS_2 nanosheets as compared to other common nanoparticles); (b) schematic illustration for the distinct redispersion behavior of 2D nanosheets and nanoparticles; (c) images illustrating the bulk redispersion of SL-MoS_2 aggregates from complete sedimentation [(1) in the absence of SRNOM; (2) post-addition to MoS_2 aggregates of 20 mg/L SRNOM; (3) co-addition to MoS_2 dispersion of 20 mg/L SRNOM]; and (d) redispersion efficiency as a function of SRNOM concentration at pH 5.0. The redispersion was initiated by replacing the supernatant with ultrapure water after centrifugation.

reversible feature of nanoparticles aggregation.[47] Even in the condition that SRNOM was post-added to the as-deposited SL-MoS_2, similar results were obtained, with the redispersion showing a much lower absorbance than the initial dispersion (Figure S9). The poor redispersion of SL-MoS_2 nanosheets is noteworthy, especially in the presence of SRNOM because NOM has been widely reported to cause the disaggregation of nanoparticles.[35,36] The distinct redispersion behavior with regarding to MoS_2 nanosheets from other reported nanoparticles might be related to their different geometric structures (2D vs 3D). For 3D nanoparticles, the disaggregation with post-addition to the aggregates of NOM is because the nanoparticle was released upon stirring (Figure 2b) and then coated by NOM, thereby preventing re-attachment to the aggregates. However, such a release could not occur in MoS_2 aggregates due to the much larger van der Waals (vdW) forces between nanosheets than that between the nanoparticles,[48] thus preventing the redispersion in post-addition to the aggregates of NOM. The geometry-dependent redispersion behavior of nanomaterials is of interest because this is the first report on the irreversible aggregation which is unique to the 2D nanosheets.

To further elucidate the role of NOM on the redispersion of SL-MoS_2 nanosheets, Figure 2c illustrates the redispersion extent of SL-MoS_2 aggregates under different SRNOM addition scenarios (i.e., co-addition and post-addition to aggregates). In contrast to the poorly redispersed aggregates in the absence or post-addition to the aggregates of SRNOM, with visible particles in the size of tens to hundreds of micrometers suspended in the solution, the deposited SL-MoS_2 could be well dispersed in the co-addition of SRNOM, transforming from the aggregated clusters to a dark brown dispersion. Furthermore, the redispersion efficiency was dependent on the SRNOM contents, with elevated efficiency as the increasing concentration of co-added SRNOM (Figure 2d). In addition, a low concentration of 5 mg/L SRNOM was used to reveal the environmental relevance, which was found to cause almost complete redispersion when the MoS_2 concentration was less than 1.6 mg/L (Figure S10). The result demonstrated the decisive role of SRNOM on the redispersion of SL-MoS_2 aggregates, which is remarkable as compared to the 3D nanoparticles. The dependence on the timing of SRNOM intervention could be attributed to the different interactions of NOM and SL-MoS_2 before and after aggregation, which will be illustrated below.

Characterization of SL-MoS_2 Aggregates as Influenced by SRNOM. To identify the structure of SL-MoS_2 aggregates and elucidate the redispersion mechanisms enabled by NOM, the aggregates formed in the absence and presence of SRNOM were subjected to a series of characterizations.

https://doi.org/10.1021/acs.est.2c05282
Environ. Sci. Technol. XXXX, XXX, XXX−XXX

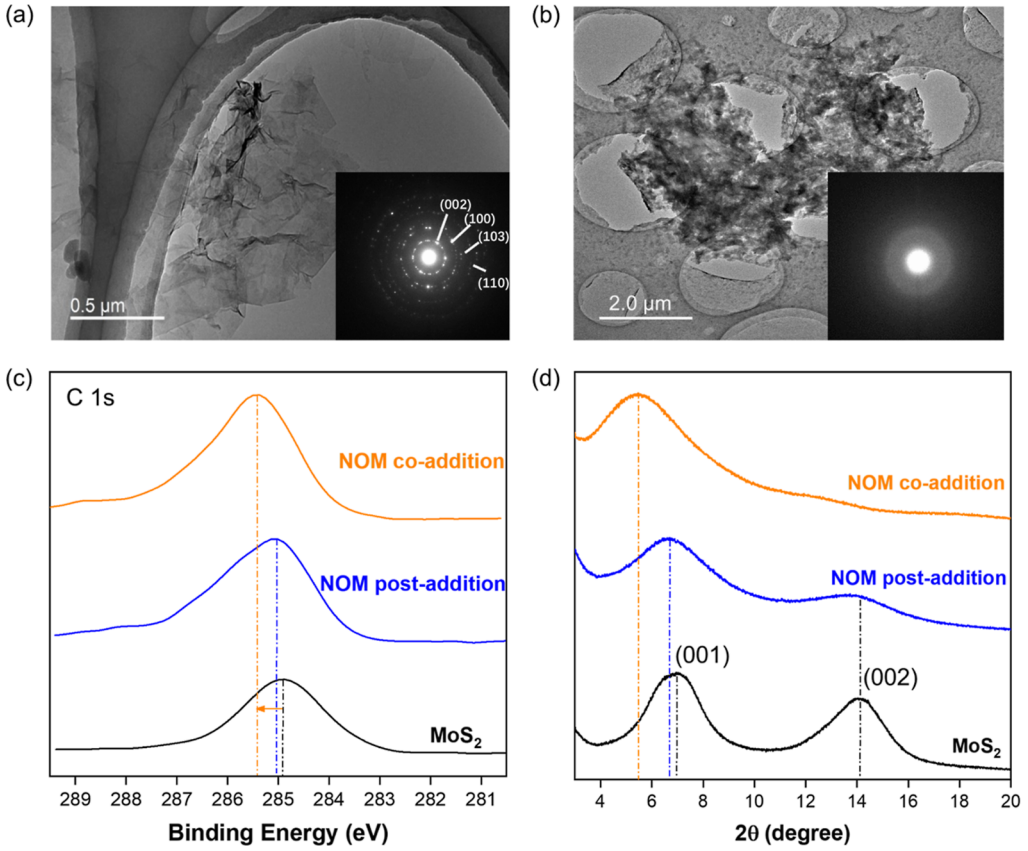

Figure 3. Characterization of the SL-MoS_2 aggregates: (a,b) representative TEM image of the aggregates formed in the absence (a) and presence (b) of SRNOM (the insets are the corresponding SAED patterns); (c) C 1s XPS spectra; and (d) X-ray diffractograms for the SL-MoS_2 aggregates formed under different conditions.

Without SRNOM, the aggregates formed with the individual nanosheet distinguishable in the TEM image (Figure 3a). Diffraction rings could be observed in the corresponding SAED pattern (Figure 3a), indicating that the aggregates were polycrystalline due to the random stacking of the SL-MoS_2 nanosheets, in contrast to the aligned MoS_2 stacks which show diffraction spots suggesting the near perfect planar structure (Figure S11). For comparison, the aggregates formed in the presence of SRNOM exhibited a flocculent morphology as evidenced by TEM imaging, and the diffusing ring in the SAED pattern suggested the amorphous structure of aggregates (Figure 3b). The energy-dispersive spectroscopy (EDS) mapping further demonstrated that elements of Mo and S from MoS_2 and C, O, and N from SRNOM were evenly distributed within the aggregates (Figure S12), confirming the sorption of SRNOM on the nanosheets. Therefore, TEM characterization revealed that the looser aggregates were formed due to the SRNOM adsorption, which could partly contribute to the easier redispersion behavior.

Besides the structure variation in the aggregates, the adsorption of SRNOM also alters the solid−water interface and leads to the disaggregation of MoS_2 nanosheets. As shown in the C 1s XPS spectra before and after SRNOM adsorption (Figure 3c), a shift to the higher binding energy could be observed in the SRNOM addition, which was resulted from the presence of C−O, C═O, and COO^- of SRNOM on the surface of MoS_2. Specifically, a larger extent of shift in the co-addition of SRNOM suggested the higher adsorption than SRNOM post-addition to the aggregates, which is consisting with the higher redispersion efficiency in the co-addition. Therefore, the presence of oxygen-containing functional groups would coordinate with water molecules to improve the nanosheet hydrophilicity and result in the enhanced hydration force. As reported in the literature, hydration force plays a dominant role to overcome the vdW attraction between the approached nanomaterials and induce the redispersion process.[49,50] To compare the amount of hydration water on the surface, the aggregated MoS_2 were subjected to filtration and then drying in the vacuum oven at 60 °C for 12 h to a constant weight. As shown in the XRD patterns (Figure 3d), the 001 peak at $2\theta = 7°$, corresponding to the d-spacing of 1.26 nm, is obvious due to the occurrence of hydrated Ca^{2+} on the surface, which is slightly higher than the d-spacing of MoS_2 (1.16 nm) in the presence of hydrated Li.[43] The 002 peak located at 14.1° was assigned to the second-order reflection of water.[51] Little difference could be observed in the post-addition to the aggregates of SRNOM, which is attributed to the negligible adsorption of SRNOM on the MoS_2 aggregates. In the co-addition of 20 mg/L SRNOM, however, the 001 peak has a left shift to ∼5.8°, suggesting the increase of d-spacing to ∼1.52 nm, which could be attributed to the presence of SRNOM and increased hydration water on the nanosheets. Therefore, the results suggested that the presence of oxygen-containing functional groups of SRNOM assisted the redispersion of MoS_2 aggregates via improving the hydrophilicity and thus enhancing the hydration force to disperse. In contrast to the NOM-induced aggregation process, where electrostatic repulsion plays a significant role,[8,32] the calculated electrostatic

https://doi.org/10.1021/acs.est.2c05282
Environ. Sci. Technol. XXXX, XXX, XXX−XXX

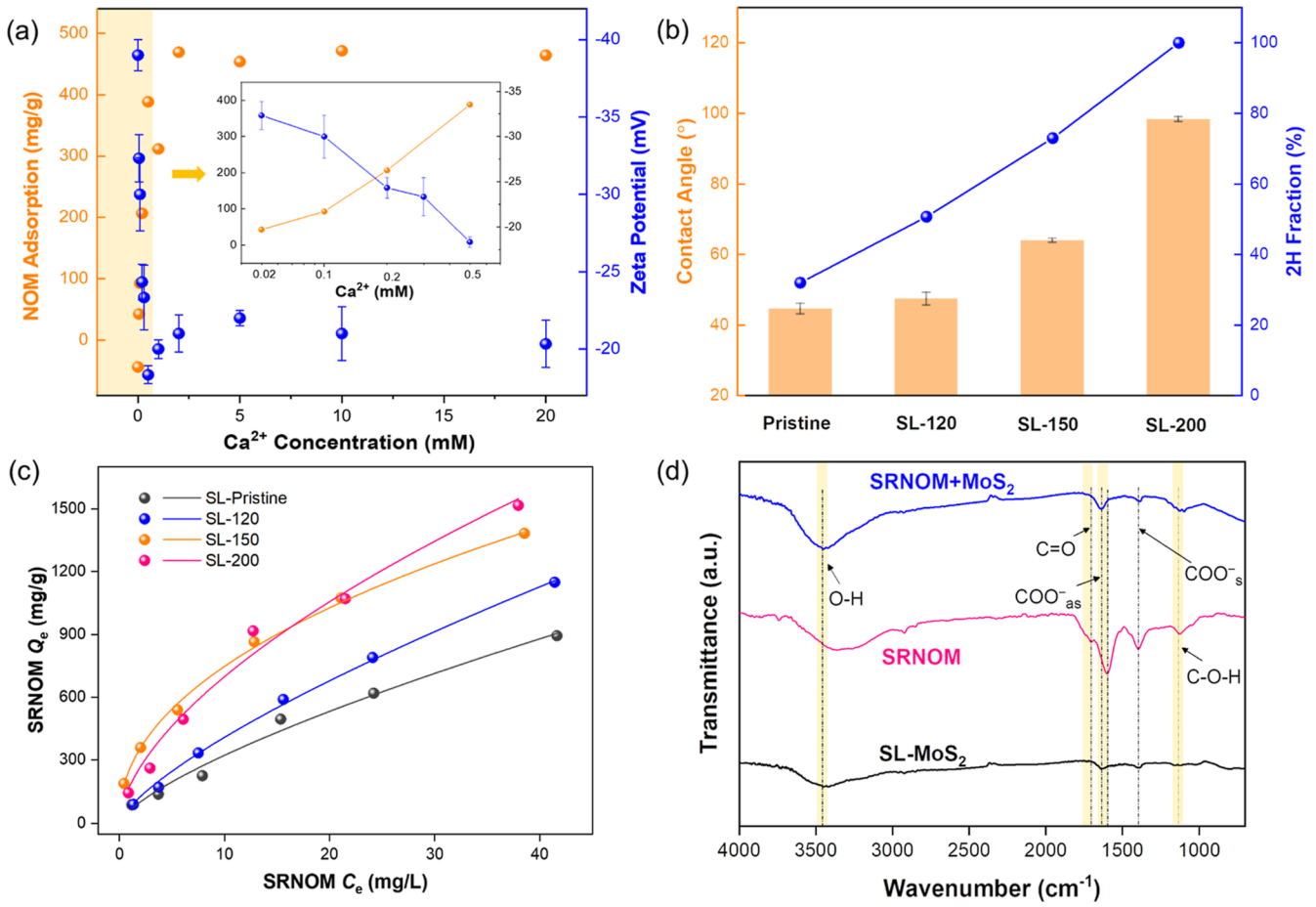

Figure 4. Adsorption of SRNOM on SL-MoS_2 surface at pH 5.0: (a) distribution coefficient (K_d) of SRNOM (left) and apparent zeta potential of SL-MoS_2 (right) as a function of Ca^{2+} concentration; (b) evolution of 2H phase fraction (right) during the transformation and water contact angles (left) of the pristine and transformed products; (c) adsorption isotherm of SRNOM on the pristine and transformed MoS_2 and fitting results by Freundlich modeling; and (d) ATR−FTIR characterization after adsorption (SRNOM and MoS_2 alone at pH 5.0 are recorded as reference).

repulsion between nanosheets in the aggregates is much lower than the vdW force even in the presence of SRNOM (Text S4). Meanwhile, the enlarged interlayer space would have weakened the vdW attractions between nanosheets, rendering easier redispersion upon adsorption of SRNOM. Overall, the changes in aggregate structure and surface properties pointed toward the necessity of elucidating the interaction mechanisms between SL-MoS_2 and SRNOM.

Interaction of SL-MoS_2, SRNOM, and Redispersion Mechanisms. Batch experiments were conducted to uncover the adsorption process of SRNOM onto SL-MoS_2 nanosheets and reveal the interaction mechanisms. Figure 4a shows the adsorption of SRNOM on SL-MoS_2 as a function of Ca^{2+} concentration. We note that the sorption did not occur without Ca^{2+} addition and the absorbance of SRNOM and SL-MoS_2 is additive (Figure S13), which could be caused by the electrostatic repulsion between highly negatively charged SL-MoS_2 and deprotonated SRNOM. The increase of Ca^{2+} concentration witnessed a rapid growth of SRNOM adsorption, and the SRNOM equilibrium sorption capacity kept a constant of ~470 mg/g at higher Ca^{2+} concentrations (2−20 mM). The increase of sorption was consistent with the dramatic decrease of SL-MoS_2 apparent zeta potential with Ca^{2+} concentration over this range in the absence of SRNOM (Figure 4a). The results suggested that the sorption was mainly initiated by electric double layer compression of SL-MoS_2 and then driven by the vdW and other attraction forces between SL-MoS_2 and SRNOM.

To further identify the attraction forces driven for the sorption, the SRNOM sorption was conducted as a function of SL-MoS_2 phase composition. We modified this by varying in the surface hydrophilicity. As the phase transformation from metallic 1T to semiconducting 2H phase, we note that the water contact angle increased from 50° of the SL-pristine to 99° of the SL-200 with pure 2H phase (Figure 4b). The results indicated the increase of hydrophobicity during transformation from metallic 1T to semiconducting 2H phase, which was consistent with the previous reports.[43,51,52] Sorption isotherms for the pristine and transformed SL-MoS_2 were obtained through altering the SRNOM concentrations in the presence of 2 mM Ca^{2+} (Figure 4c). The sorption could be well fitted by the Freundlich model, with R^2 no less than 0.98 (Table S1). Compared to the SL-pristine, higher sorption of SRNOM was observed in the phase-transformed nanosheets. In the addition of 50 mg/L SRNOM, for example, the equilibrium adsorption capacity increased from 893 mg/g of the SL-pristine to 1149, 1382, and 1516 mg/g of the SL-120, -150, and -200, respectively. The results suggested that the semiconducting 2H phase with relatively more hydrophobic surface possesses stronger affinity to SRNOM compared to the 1T phase, which implied that the sorption of SRNOM was driven by the hydrophobic moieties of SRNOM. After adsorption to SL-

https://doi.org/10.1021/acs.est.2c05282
Environ. Sci. Technol. XXXX, XXX, XXX−XXX

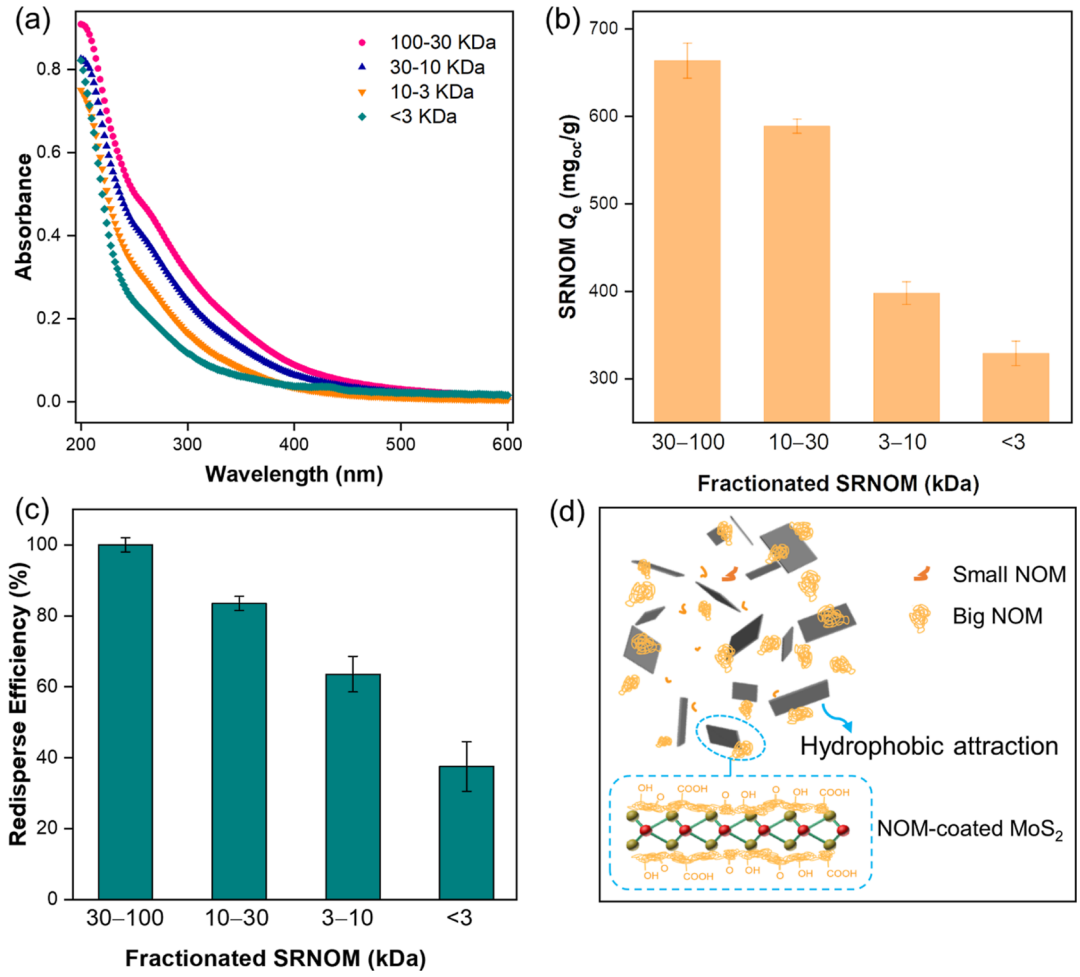

Figure 5. Characterization and role of MW-fractionated SRNOM (<3, 3−10, 10−30, and 30−100 kDa): (a) UV−vis absorbance (10 mg_{oc}/L); (b) adsorption capacity of SL-MoS_2 for MW-fractionated SRNOM at pH 5.0 (the total addition of fractionated SRNOM is 20 mg_{oc}/L); (c) redispersion efficiencies at pH 5.0 for the aggregates induced by 2 mM Ca^{2+} with the addition of fractionated SRNOM in 20 mg_{oc}/L; and (d) proposed interaction mechanisms of SRNOM and MoS_2.

pristine, we noticed that the spectra ratio (S_R, slope of 275−295 nm region: slope of 350−400 region) of SRNOM increased from 0.71 to 0.77 (Figure S14), suggesting the decreased MW of SRNOM due to the adsorption.[53] The results could be attributed to the preferable adsorption for the fraction with higher MW, which needs further examination in the following. With respect to the previous studies, most of them discussed the sorption of NOM to nanomaterials with positive charge via electrostatic attraction or organic nanomaterials via $\pi-\pi$ interaction. Our results filled the gap by providing mechanistic new insights into the sorption of NOM on inorganic nanomaterials with negative surface charge, which could represent a large proportion of engineered nanomaterials. Post-adsorption of SRNOM on MoS_2 aggregates is much lower than the adsorption on the nanosheets (Figure S15), which could explain the poor dispersity and limited exposed surface area of MoS_2 aggregates in the post-addition to the aggregates of SRNOM (Figure 2b).

Besides Ca^{2+}, other cations such as Na^+ could also induce the sorption of SRNOM on SL-MoS_2 by the similar mechanisms, with a rapid increase of SRNOM adsorption by increasing Na^+ concentrations (Figure S16a). However, the Na^+ concentration required (30 mM) for the maximum adsorption is much higher than that of Ca^{2+} (2 mM), which could be explained by the lower destabilization ability of monovalent cations.[28,30,54] Regarding the case in the presence of Na^+, we note that a higher redispersion efficiency was obtained at each concentration of SRNOM (Figure S16b) than that in the solution containing Ca^{2+} despite the sorption being much lower (Figure S16a). Correspondingly, the average hydrodynamic diameter of the redispersion is much smaller in Na-induced aggregates (Figure S16c). The results indicated the easier redispersion from Na-induced aggregates, which could be resulted from the more extended structure of SRNOM on MoS_2 surface than that in Ca^{2+} addition (Figure S16d). As reported, the presence of Ca^{2+} could induce the self-association of SRNOM through ionic bridging effects,[55,56] thus existing as the relatively condense structure on the surface of nanosheets.

ATR−FTIR spectroscopy of the SRNOM in the 500−4000 cm^{-1} region was compared after adsorption onto SL-MoS_2 (Figure 4d). Spectra on SRNOM alone and SL-MoS_2 alone at pH 5.0 were recorded as references. Changes in the following vibration bands were monitored:[57−59] the disappearance of C═O at 1710 cm^{-1} from carboxylic acid and phenolic C−OH at 1134 cm^{-1} might result from the deprotonation of SRNOM for ligand exchange, as the reported phenomenon of NOM adsorption on ferrihydrite;[15] a shift from 1593 to 1640 cm^{-1} of

https://doi.org/10.1021/acs.est.2c05282
Environ. Sci. Technol. XXXX, XXX, XXX−XXX

COO^- after adsorption could be ascribed to preferential complexation of Ca^{2+} with carboxylic sites on the SRNOM.[60] Upon adsorption, the hydroxyl bond stretching at 3450 cm^{-1} of SL-MoS_2 was enhanced, indicating the affinity of water molecules to the nanosheets was improved due to the sorption of SRNOM,[58] thus leading to the better dispersibility of SL-MoS_2.

Effects of Fractionated SRNOM on Aggregation and Redispersion. Based on the interaction mechanisms proposed, we hypothesize that the SRNOM with higher aromaticity and thus hydrophobicity would exhibit stronger adsorption onto SL-MoS_2 in the presence of cations. To verify this hypothesis and gain further insights into the effects of NOM properties on the adsorption-redispersion behavior of MoS_2, SRNOM was fractionated into fractions with different molecular masses. The successful sequential fractionation of SRNOM could be confirmed by the UV−vis absorbance normalized to the carbon content (Figure 5a). The higher absorbance of at the UV region (200−400 nm) as the increase of molecular mass indicated that the aromatic components and more hydrophobic structures existed mainly in the fraction with higher molecular mass.[18,34] Furthermore, fluorescence EEM analysis were utilized to unravel the compositional differences in fractionated SRNOM. All fractions of SRNOM showed spectra peaks at the excitation/emission wavelengths (Ex/Em) of 464−468/433−474 (Figure S17), which could be assigned to humic-acid-like organics.[61] With the increase of molecular mass, the general decreasing fluorescence maximum intensities suggested the decreasing abundance of carboxylic functional groups.[62] We noted a red shift of Em maxima with the increase in molecular mass, which was consistent with literature owing to the rising abundance of aromatic chromophores.[16] Therefore, the EEM characterization coupling with the UV−vis spectra suggested the preferable occurrences of aromatic components in big molecules of SRNOM, while carboxylic groups in the fraction with low molecular mass.

As expected, the addition of fractionated SRNOM with same carbon concentration displayed distinguished stabilizing effects on SL-MoS_2 (Figure S18). Specifically, the aggregation rate induced by 200 mM Na^+ decreased from 0.72 nm/s without SRNOM to 0.59, 0.38, 0.06, and 0.01 nm/s by the presence of SRNOM fraction (2 mg_{oc}/L) of <3, 3−10, 10−30, and 30−100 kDa, respectively. The results are consistent with the previous reports,[16,17,63] suggesting stronger stabilizing effects due to the more profound hindrances from larger NOM molecules. In the process of aggregation, the amount of SRNOM adsorbed onto SL-MoS_2 was quantified by the TOC measurement before and after adsorption. As shown in Figure 5b, the amount of SRNOM sorption is positively correlated to the molecular mass of fractionated SRNOM. The results demonstrated the preferable adsorption of the SRNOM fraction with higher molecular mass. We attributed this to the higher amount of aromatic and hydrophobic compounds in the high molecular mass fraction and further confirmed the dominant contribution from hydrophobic moieties of SRNOM. Correspondingly, the redispersion efficiency also increased as the molecular mass of SRNOM due to the preferable adsorption of high molecular mass fraction (Figure 5c).

Overall, the interaction of SL-MoS_2 and SRNOM could be summarized as follows (Figure 5d). In the solution containing cations, SL-MoS_2 nanosheets were subjected to aggregation, which accompanied by the adsorption of SRNOM, especially the large molecules, onto the nanosheets. The elevated redispersion was achieved by the simultaneously enhanced hydration repulsion force and weakened vdW attractions: first, the oxygen functional groups introduced on the surface improved the hydrophilicity and thus hydration force required for redispersion; for another, due to intercalation of NOM into the aggregates, the vdW forces would be inevitably weakened by the enlarged interlayer spacing. We note that the later mechanism of NOM action is specific to 2D nanosheets and relies on the timing of NOM presence, which could only occur in the NOM co-addition to Ca^{2+} scenario rather than the post-addition that the interlayer spacing of as-deposited SL-MoS_2 is too narrow to allow the intercalation of the NOM molecules.

■ ENVIRONMENTAL IMPLICATIONS

The aggregation and redispersion behavior of nanomaterials, particularly in natural systems, is an important consideration in determining their mobility and persistence, as well as toxicity. This study presented a systematic investigation on the NOM-influenced aggregation and redispersion behavior of 2D MoS_2 nanosheets. The aggregate structure, morphology, and interfacial properties are altered upon interaction with NOM, and the results implied that the presence of NOM would remobilize the aggregates depending on the timing of NOM presence. For instance, post-presence of SRNOM could not elute the as-deposited MoS_2 in the sand column; however, when the aggregates formed in the presence of SRNOM were deposited in the quartz sand column (Text S3), an increasing amount of SL-MoS_2 nanosheets was recovered in the effluent as the increase of SRNOM contents (Figure 6). The special

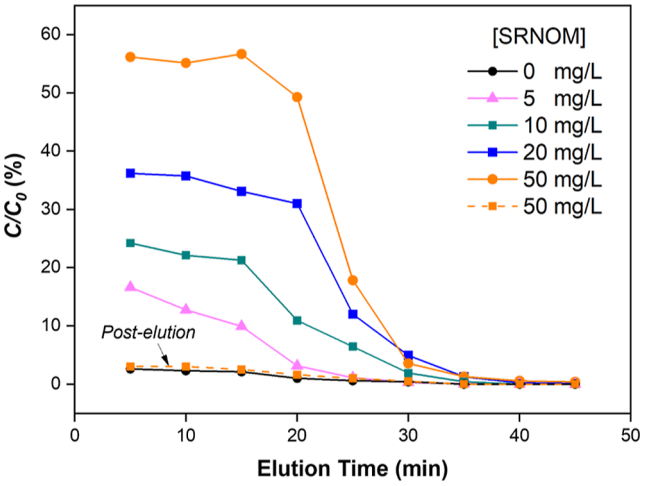

Figure 6. Recovery of MoS_2 in the effluent of the column (the MoS_2 aggregates was formed with the addition of 2 mM Ca^{2+} and a series of SRNOM solutions at concentrations from 0 to 50 mg/L). The dashed line denotes the post-elution of 50 mg/L SRNOM for as-deposited MoS_2.

dependence on the timing of interventions (e.g., adsorption of NOM) emphasized the distinguished behavior of 2D nanosheets from the well-researched 3D nanoparticles. This observation implies that the transformation of 2D nanomaterials should have more privileged discussion. Based on the interaction mechanisms, we would expect the nanosheets obtained by other cleaving methods such as ultrasonication and electrochemical exfoliation that are dominant in the 2H

https://doi.org/10.1021/acs.est.2c05282
Environ. Sci. Technol. XXXX, XXX, XXX−XXX

phase would display higher adsorption to NOM. Moreover, NOM from different origins should be taken into consideration in future studies. For example, the NOM in groundwater often consists of compounds with higher hydrogen−carbon ratio (H/C) and lower O/C, such as some amino acids, sugars, lipids, and complex organics as compared to that from the surface water (e.g., river water, estuarine water, etc.),[64] which is expected display higher adsorption on MoS_2 nanosheets.

■ ASSOCIATED CONTENT

Supporting Information

The Supporting Information is available free of charge at https://pubs.acs.org/doi/10.1021/acs.est.2c05282.

Chemical reagents, additional information on the preparation of SL-MoS_2 nanosheets, column experiment, calculation of electrostatic repulsion and vdW attraction energy, characterization of the flower-like MoS_2 nanoparticle, zeta potentials, sedimentation profile, linear correlation of absorbance at 450 nm to concentration of SL-MoS_2 redispersion, illustration of NOM co-addition and post-addition, adsorption and post-adsorption kinetics, characterization of transformed SL-MoS_2 dispersion, UV−vis spectra, redispersion efficiency, TEM image, EDS mapping, absorbance spectra, adsorption and post-adsorption isotherms, fluorescence EEMs, influence of fractionated SRNOM, and Freundlich fitting parameters (PDF)

■ AUTHOR INFORMATION

Corresponding Authors

Zhongying Wang − *School of Environmental Science and Engineering, Southern University of Science and Technology, Shenzhen 518055, China;* orcid.org/0000-0002-7869-6859; Email: wangzy6@sustech.edu.cn

[§]**Joel A. Pedersen** − *Department of Environmental Health and Engineering, Johns Hopkins University, Baltimore, Maryland 21218, United States*; Email: jpeders9@jhu.edu

Authors

Bei Liu − *School of Environmental Science and Engineering, Southern University of Science and Technology, Shenzhen 518055, China*

Zixin Han − *School of Environmental Science and Engineering, Southern University of Science and Technology, Shenzhen 518055, China*

Qi Han − *School of Environmental Science and Engineering, Southern University of Science and Technology, Shenzhen 518055, China*

Yufei Shu − *School of Environmental Science and Engineering, Southern University of Science and Technology, Shenzhen 518055, China*

Li Li − *School of Environmental Science and Engineering, Southern University of Science and Technology, Shenzhen 518055, China*

Beizhao Chen − *School of Environmental Science and Engineering, Southern University of Science and Technology, Shenzhen 518055, China*

Complete contact information is available at: https://pubs.acs.org/10.1021/acs.est.2c05282

Notes

The authors declare no competing financial interest.

[§]Passed away on June 29, 2022.

■ ACKNOWLEDGMENTS

We would like to dedicate this paper to the memory of our coauthor and dear friend J.A.P., who passed away during the paper revision. His contributions to the environmental nanotechnology and environmental chemistry communities will be long remembered. We will remain grateful to Dr. Pedersen for sharing with us his technical expertise and enthusiasm for research and life. This work was financially supported by the National Natural Science Foundation of China (nos. 41907296 and 22076075). The contributions of J.A.P. were supported by the National Science Foundation under the NSF Center for Sustainable Nanotechnology, CHE-2001611. The authors acknowledge the assistance of SUSTech Core Research Facilities.

■ REFERENCES

(1) Midya, A.; Ghorai, A.; Mukherjee, S.; Maiti, R.; Ray, S. K. Hydrothermal Growth of Few Layer 2H-MoS_2 for Heterojunction Photodetector and Visible Light Induced Photocatalytic Applications. *J. Mater. Chem. A* **2016**, *4*, 4534−4543.

(2) Lukowski, M. A.; Daniel, A. S.; Meng, F.; Forticaux, A.; Li, L.; Jin, S. Enhanced Hydrogen Evolution Catalysis from Chemically Exfoliated Metallic MoS_2 Nanosheets. *J. Am. Chem. Soc.* **2013**, *135*, 10274−10277.

(3) Liu, T.; Wang, C.; Gu, X.; Gong, H.; Cheng, L.; Shi, X.; Feng, L.; Sun, B.; Liu, Z. Drug Delivery with PEGylated MoS_2 Nano-Sheets for Combined Photothermal and Chemotherapy of Cancer. *Adv. Mater.* **2014**, *26*, 3433−3440.

(4) Lembke, D.; Bertolazzi, S.; Kis, A. Single-Layer MoS_2 Electronics. *Acc. Chem. Res.* **2015**, *48*, 100−110.

(5) Shi, Z. T.; Kang, W.; Xu, J.; Sun, Y. W.; Jiang, M.; Ng, T. W.; Xue, H. T.; Yu, D. Y. W.; Zhang, W.; Lee, C. S. Hierarchical Nanotubes Assembled from MoS_2-Carbon Monolayer Sandwiched Superstructure Nanosheets for High-Performance Sodium Ion Batteries. *Nano Energy* **2016**, *22*, 27−37.

(6) Lowry, G. V.; Gregory, K. B.; Apte, S. C.; Lead, J. R. Transformations of Nanomaterials in the Environment. *Environ. Sci. Technol.* **2012**, *46*, 6893−6899.

(7) Hochella, M. F.; Mogk, D. W.; Ranville, J.; Allen, I. C.; Luther, G. W.; Marr, L. C.; McGrail, B. P.; Murayama, M.; Qafoku, N. P.; Rosso, K. M.; Sahai, N.; Schroeder, P. A.; Vikesland, P.; Westerhoff, P.; Yang, Y. Natural, Incidental, and Engineered Nanomaterials and Their Impacts on the Earth System. *Science* **2019**, *363*, No. eaau8299.

(8) Lee, T. W.; Chen, C. C.; Chen, C. Chemical Stability and Transformation of Molybdenum Disulfide Nanosheets in Environmental Media. *Environ. Sci. Technol.* **2019**, *53*, 6282−6291.

(9) Lowry, G. V.; Hotze, E. M.; Bernhardt, E. S.; Dionysiou, D. D.; Pedersen, J. A.; Wiesner, M. R.; Xing, B. Environmental Occurrences, Behavior, Fate, and Ecological Effects of Nanomaterials: An Introduction to the Special Series. *J. Environ. Qual.* **2010**, *39*, 1867.

(10) Yi, P.; Chen, K. L. Release Kinetics of Multiwalled Carbon Nanotubes Deposited on Silica Surfaces: Quartz Crystal Microbalance with Dissipation (QCM-D) Measurements and Modeling. *Environ. Sci. Technol.* **2014**, *48*, 4406−4413.

(11) Sutton, R.; Sposito, G. Molecular Structure in Soil Humic Substances: The New View. *Environ. Sci. Technol.* **2005**, *39*, 9009−9015.

(12) Zark, M.; Dittmar, T. Universal Molecular Structures in Natural Dissolved Organic Matter. *Nat. Commun.* **2018**, *9*, 3178.

(13) Hotze, E. M.; Phenrat, T.; Lowry, G. V. Nanoparticle Aggregation: Challenges to Understanding Transport and Reactivity in the Environment. *J. Environ. Qual.* **2010**, *39*, 1909.

(14) Mensch, A. C.; Hernandez, R. T.; Kuether, J. E.; Torelli, M. D.; Feng, Z. V.; Hamers, R. J.; Pedersen, J. A. Natural Organic Matter Concentration Impacts the Interaction of Functionalized Diamond Nanoparticles with Model and Actual Bacterial Membranes. *Environ. Sci. Technol.* **2017**, *51*, 11075−11084.
(15) Li, Z.; Shakiba, S.; Deng, N.; Chen, J.; Louie, S. M.; Hu, Y. Natural Organic Matter (NOM) Imparts Molecular-Weight-Dependent Steric Stabilization or Electrostatic Destabilization to Ferrihydrite Nanoparticles. *Environ. Sci. Technol.* **2020**, *54*, 6761−6770.
(16) Shen, M. H.; Yin, Y. G.; Booth, A.; Liu, J. F. Effects of Molecular Weight-Dependent Physicochemical Heterogeneity of Natural Organic Matter on the Aggregation of Fullerene Nanoparticles in Mono- and Di-Valent Electrolyte Solutions. *Water Res.* **2015**, *71*, 11−20.
(17) Louie, S. M.; Tilton, R. D.; Lowry, G. V. Effects of Molecular Weight Distribution and Chemical Properties of Natural Organic Matter on Gold Nanoparticle Aggregation. *Environ. Sci. Technol.* **2013**, *47*, 4245−4254.
(18) Yin, Y.; Shen, M.; Tan, Z.; Yu, S.; Liu, J.; Jiang, G. Particle Coating-Dependent Interaction of Molecular Weight Fractionated Natural Organic Matter: Impacts on the Aggregation of Silver Nanoparticles. *Environ. Sci. Technol.* **2015**, *49*, 6581−6589.
(19) Deng, N.; Li, Z.; Zuo, X.; Chen, J.; Shakiba, S.; Louie, S. M.; Rixey, W. G.; Hu, Y. Coprecipitation of Fe/Cr Hydroxides with Organics: Roles of Organic Properties in Composition and Stability of the Coprecipitates. *Environ. Sci. Technol.* **2021**, *55*, 4638−4647.
(20) Philippe, A.; Schaumann, G. E. Interactions of Dissolved Organic Matter with Natural and Engineered Inorganic Colloids: A Review. *Environ. Sci. Technol.* **2014**, *48*, 8946−8962.
(21) Hyung, H.; Kim, J. H. Natural Organic Matter (NOM) Adsorption to Multi-Walled Carbon Nanotubes: Effect of NOM Characteristics and Water Quality Parameters. *Environ. Sci. Technol.* **2008**, *42*, 4416−4421.
(22) Wang, D.; Yue, J.; Cui, D.; Zhang, L.; Dong, X. Insights into Adsorption of Humic Substances on Graphitic Carbon Nitride. *Environ. Sci. Technol.* **2021**, *55*, 7910−7919.
(23) Smith, B.; Yang, J.; Bitter, J. L.; Ball, W. P.; Fairbrother, D. H. Influence of Surface Oxygen on the Interactions of Carbon Nanotubes with Natural Organic Matter. *Environ. Sci. Technol.* **2012**, *46*, 12839−12847.
(24) Shakiba, S.; Hakimian, A.; Barco, L. R.; Louie, S. M. Dynamic Intermolecular Interactions Control Adsorption from Mixtures of Natural Organic Matter and Protein onto Titanium Dioxide Nanoparticles. *Environ. Sci. Technol.* **2018**, *52*, 14158−14168.
(25) Shang, E.; Li, Y.; Niu, J.; Zhou, Y.; Wang, T.; Crittenden, J. C. Relative Importance of Humic and Fulvic Acid on ROS Generation, Dissolution, and Toxicity of Sulfide Nanoparticles. *Water Res.* **2017**, *124*, 595−604.
(26) Franchi, A.; O'Melia, C. R. Effects of Natural Organic Matter and Solution Chemistry on the Deposition and Reentrainment of Colloids in Porous Media. *Environ. Sci. Technol.* **2003**, *37*, 1122−1129.
(27) Ha, Y.; Wang, X.; Liljestrand, H. M.; Maynard, J. A.; Katz, L. E. Bioavailability of Fullerene under Environmentally Relevant Conditions: Effects of Humic Acid and Fetal Bovine Serum on Accumulation in Lipid Bilayers and Cellular Uptake. *Environ. Sci. Technol.* **2016**, *50*, 6717−6727.
(28) Liu, B.; Han, Q.; Li, L.; Zheng, S.; Shu, Y.; Pedersen, J. A.; Wang, Z. Synergistic Effect of Metal Cations and Visible Light on 2D MoS_2 Nanosheet Aggregation. *Environ. Sci. Technol.* **2021**, *55*, 16379−16389.
(29) Zou, W.; Zhou, Q.; Zhang, X.; Hu, X. Dissolved Oxygen and Visible Light Irradiation Drive the Structural Alterations and Phytotoxicity Mitigation of Single-Layer Molybdenum Disulfide. *Environ. Sci. Technol.* **2019**, *53*, 7759−7769.
(30) Mohona, T. M.; Gupta, A.; Masud, A.; Chien, S. C.; Lin, L. C.; Nalam, P. C.; Aich, N. Aggregation Behavior of Inorganic 2D Nanomaterials beyond Graphene: Insights from Molecular Modeling and Modified DLVO Theory. *Environ. Sci. Technol.* **2019**, *53*, 4161−4172.
(31) Zou, W.; Zhou, Q.; Zhang, X.; Hu, X. Environmental Transformations and Algal Toxicity of Single-Layer Molybdenum Disulfide Regulated by Humic Acid. *Environ. Sci. Technol.* **2018**, *52*, 2638−2648.
(32) Sabaraya, I. V.; Shin, H.; Li, X.; Hoq, R.; Incorvia, J. A. C.; Kirisits, M. J.; Saleh, N. B. Role of Electrostatics in the Heterogeneous Interaction of Two-Dimensional Engineered MoS_2 Nanosheets and Natural Clay Colloids: Influence of PH and Natural Organic Matter. *Environ. Sci. Technol.* **2021**, *55*, 919−929.
(33) Johnson, S. B.; Brown, G. E.; Healy, T. W.; Scales, P. J. Adsorption of Organic Matter at Mineral/Water Interfaces. 6. Effect of Inner-Sphere versus Outer-Sphere Adsorption on Colloidal Stability. *Langmuir* **2005**, *21*, 6356−6365.
(34) Shen, Z.; Zhang, Z.; Li, T.; Yao, Q.; Zhang, T.; Chen, W. Facet-Dependent Adsorption and Fractionation of Natural Organic Matter on Crystalline Metal Oxide Nanoparticles. *Environ. Sci. Technol.* **2020**, *54*, 8622−8631.
(35) Loosli, F.; Le Coustumer, P.; Stoll, S. Effect of Natural Organic Matter on the Disagglomeration of Manufactured TiO_2 Nanoparticles. *Environ. Sci.: Nano* **2014**, *1*, 154−160.
(36) Baalousha, M. Aggregation and Disaggregation of Iron Oxide Nanoparticles: Influence of Particle Concentration, PH and Natural Organic Matter. *Sci. Total Environ.* **2009**, *407*, 2093−2101.
(37) Koh, B.; Cheng, W. Mechanisms of Carbon Nanotube Aggregation and the Reversion of Carbon Nanotube Aggregates in Aqueous Medium. *Langmuir* **2014**, *30*, 10899−10909.
(38) Eda, G.; Yamaguchi, H.; Voiry, D.; Fujita, T.; Chen, M.; Chhowalla, M. Photoluminescence from Chemically Exfoliated MoS_2. *Nano Lett.* **2011**, *11*, 5111−5116.
(39) Wang, Z.; Zhang, Y. J.; Liu, M.; Peterson, A.; Hurt, R. H. Oxidation Suppression during Hydrothermal Phase Reversion Allows Synthesis of Monolayer Semiconducting MoS_2 in Stable Aqueous Suspension. *Nanoscale* **2017**, *9*, 5398−5403.
(40) Han, Q.; Cao, H.; Sun, Y.; Wang, G.; Poon, S.; Wang, M.; Liu, B.; Wang, Y.; Wang, Z.; Mi, B. Tuning Phase Compositions of MoS_2 Nanomaterials for Enhanced Heavy Metal Removal: Performance and Mechanism. *Phys. Chem. Chem. Phys.* **2022**, *24*, 13305−13316.
(41) Rosario-Ortiz, F. L.; Snyder, S.; Suffet, I. H. Characterization of the Polarity of Natural Organic Matter under Ambient Conditions by the Polarity Rapid Assessment Method (PRAM). *Environ. Sci. Technol.* **2007**, *41*, 4895−4900.
(42) Voiry, D.; Salehi, M.; Silva, R.; Fujita, T.; Chen, M.; Asefa, T.; Shenoy, V. B.; Eda, G.; Chhowalla, M. Conducting MoS_2 Nanosheets as Catalysts for Hydrogen Evolution Reaction. *Nano Lett.* **2013**, *13*, 6222−6227.
(43) Ries, L.; Petit, E.; Michel, T.; Diogo, C. C.; Gervais, C.; Salameh, C.; Bechelany, M.; Balme, S.; Miele, P.; Onofrio, N.; Voiry, D. Enhanced Sieving from Exfoliated MoS_2 Membranes via Covalent Functionalization. *Nat. Mater.* **2019**, *18*, 1112−1117.
(44) Heising, J.; Kanatzidis, M. G. Exfoliated and Restacked MoS_2 and WS_2: Ionic or Neutral Species? Encapsulation and Ordering of Hard Electropositive Cations. *J. Am. Chem. Soc.* **1999**, *121*, 11720−11732.
(45) Guardia, L.; Paredes, J. I.; Munuera, J. M.; Villar-Rodil, S.; Ayán-Varela, M.; Martínez-Alonso, A.; Tascón, J. M. D. Chemically Exfoliated MoS_2 Nanosheets as an Efficient Catalyst for Reduction Reactions in the Aqueous Phase. *ACS Appl. Mater. Interfaces* **2014**, *6*, 21702−21710.
(46) Wang, Z.; von dem Bussche, A.; Qiu, Y.; Valentin, T. M.; Gion, K.; Kane, A. B.; Hurt, R. H. Chemical Dissolution Pathways of MoS_2 Nanosheets in Biological and Environmental Media. *Environ. Sci. Technol.* **2016**, *50*, 7208−7217.
(47) Sokolov, S. V.; Tschulik, K.; Batchelor-McAuley, C.; Jurkschat, K.; Compton, R. G. Reversible or Not? Distinguishing Agglomeration and Aggregation at the Nanoscale. *Anal. Chem.* **2015**, *87*, 10033−10039.

https://doi.org/10.1021/acs.est.2c05282
Environ. Sci. Technol. XXXX, XXX, XXX−XXX

(48) Liu, B.; Han, Z.; Han, Q.; Shu, Y.; Wang, M.; Wang, L.; Wang, Z.; Pedersen, J. A. Emerging Investigator Series: Correlating Phase Composition and Geometric Structure to the Colloidal Stability of 2D MoS_2 Nanomaterials. *Environ. Sci.: Nano* **2022**, *9*, 1605−1616.
(49) Desset, S.; Spalla, O.; Cabane, B. Redispersion of Alumina Particles in Water. *Langmuir* **2000**, *16*, 10495−10508.
(50) Sharma, M. M.; Chamoun, H.; Sarma, D. S. H. S. R.; Schechter, R. S. Factors Controlling the Hydrodynamic Detachment of Particles from Surfaces. *J. Colloid Interface Sci.* **1992**, *149*, 121−134.
(51) Geng, X.; Sun, W.; Wu, W.; Chen, B.; Al-Hilo, A.; Benamara, M.; Zhu, H.; Watanabe, F.; Cui, J.; Chen, T. P. Pure and Stable Metallic Phase Molybdenum Disulfide Nanosheets for Hydrogen Evolution Reaction. *Nat. Commun.* **2016**, *7*, 10672.
(52) Acerce, M.; Voiry, D.; Chhowalla, M. Metallic 1T phase MoS2 nanosheets as supercapacitor electrode materials. *Nat. Nanotechnol.* **2015**, *10*, 313−318.
(53) Helms, J. R.; Stubbins, A.; Ritchie, J. D.; Minor, E. C.; Kieber, D. J.; Mopper, K. Erratum: Absorption Spectral Slopes and Slope Ratios as Indicators of Molecular Weight, Source, and Photobleaching of Chromophoric Dissolved Organic Matter. *Limnol. Oceanogr.* **2009**, *54*, 1023.
(54) Yang, K.; Chen, B.; Zhu, X.; Xing, B. Aggregation, Adsorption, and Morphological Transformation of Graphene Oxide in Aqueous Solutions Containing Different Metal Cations. *Environ. Sci. Technol.* **2016**, *50*, 11066−11075.
(55) Mylon, S. E.; Chen, K. L.; Elimelech, M. Influence of Natural Organic Matter and Ionic Composition on the Kinetics and Structure of Hematite Colloid Aggregation: Implications to Iron Depletion in Estuaries. *Langmuir* **2004**, *20*, 9000−9006.
(56) Avena, M. J.; Wilkinson, K. J. Disaggregation Kinetics of a Peat Humic Acid: Mechanism and PH Effects. *Environ. Sci. Technol.* **2002**, *36*, 5100−5105.
(57) Aristilde, L.; Marichal, C.; Miéhé-Brendlé, J.; Lanson, B.; Charlet, L. Interactions of Oxytetracycline with a Smectite Clay: A Spectroscopic Study with Molecular Simulations. *Environ. Sci. Technol.* **2010**, *44*, 7839−7845.
(58) Zheng, S.; Tu, Q.; Urban, J. J.; Li, S.; Mi, B. Swelling of Graphene Oxide Membranes in Aqueous Solution: Characterization of Interlayer Spacing and Insight into Water Transport Mechanisms. *ACS Nano* **2017**, *11*, 6440−6450.
(59) Zhang, X.; Graham, N.; Xu, L.; Yu, W.; Gregory, J. The Influence of Small Organic Molecules on Coagulation from the Perspective of Hydrolysis Competition and Crystallization. *Environ. Sci. Technol.* **2021**, *55*, 7456−7465.
(60) Christl, I. Ionic Strength- and PH-Dependence of Calcium Binding by Terrestrial Humic Acids. *Environ. Chem.* **2012**, *9*, 89.
(61) Chen, W.; Westerhoff, P.; Leenheer, J. A.; Booksh, K. Fluorescence Excitation−Emission Matrix Regional Integration to Quantify Spectra for Dissolved Organic Matter. *Environ. Sci. Technol.* **2003**, *37*, 5701−5710.
(62) Richard, C.; Guyot, G.; Rivaton, A.; Trubetskaya, O.; Trubetskoj, O.; Cavani, L.; Ciavatta, C. Spectroscopic Approach for Elucidation of Structural Peculiarities of Andisol Soil Humic Acid Fractionated by SEC-PAGE Setup. *Geoderma* **2007**, *142*, 210−216.
(63) Louie, S. M.; Spielman-Sun, E. R.; Small, M. J.; Tilton, R. D.; Lowry, G. V. Correlation of the Physicochemical Properties of Natural Organic Matter Samples from Different Sources to Their Effects on Gold Nanoparticle Aggregation in Monovalent Electrolyte. *Environ. Sci. Technol.* **2015**, *49*, 2188−2198.
(64) McDonough, L. K.; Andersen, M. S.; Behnke, M. I.; Rutlidge, H.; Oudone, P.; Meredith, K.; O'Carroll, D. M.; Santos, I. R.; Marjo, C. E.; Spencer, R. G. M.; McKenna, A. M.; Baker, A. A New Conceptual Framework for the Transformation of Groundwater Dissolved Organic Matter. *Nat. Commun.* **2022**, *13*, 2153.

https://doi.org/10.1021/acs.est.2c05282
Environ. Sci. Technol. XXXX, XXX, XXX−XXX